Thermodynamic Evidence of Fermionic Behavior in the Vicinity of One-Ninth Plateau in a Kagome Antiferromagnet

Guoxin Zheng,[1] Dechen Zhang,[1] Yuan Zhu,[1] Kuan-Wen Chen,[1] Aaron Chan,[1] Kaila Jenkins,[1] Byungmin Kang,[2] Zhenyuan Zeng,[3,4] Aini Xu,[3,4] D. Ratkovski,[5] Joanna Blawat,[6] Alimamy F. Bangura,[5] John Singleton,[6] Patrick A. Lee,[2] Shiliang Li,[3,4,7] and Lu Li[1,*]

[1]Department of Physics, University of Michigan, Ann Arbor, Michigan 48109, USA
[2]Department of Physics, Massachusetts Institute of Technology, Cambridge, Massachusetts 02139, USA
[3]Beijing National Laboratory for Condensed Matter Physics, Institute of Physics, Chinese Academy of Sciences, Beijing 100190, China
[4]School of Physical Sciences, University of Chinese Academy of Sciences, Beijing, 100190, China
[5]National High Magnetic Field Laboratory, 1800 East Paul Dirac Drive, Tallahassee, Florida 32310-3706, USA
[6]National High Magnetic Field Laboratory, MS E536, Los Alamos National Laboratory, Los Alamos, New Mexico 87545, USA
[7]Songshan Lake Materials Laboratory, Dongguan, Guangdong, 523808, China

(Received 8 September 2024; revised 17 December 2024; accepted 1 May 2025; published 30 May 2025)

The spin-1/2 kagome Heisenberg antiferromagnets are believed to host exotic quantum entangled states. Recently, the reports of 1/9 magnetization plateau and magnetic oscillations in a kagome antiferromagnet $YCu_3(OH)_6Br_2[Br_x(OH)_{1-x}]$ (YCOB) have made this material a promising candidate for experimentally realizing quantum spin liquid states. Here, we present measurements of the specific heat C_p in YCOB in high magnetic fields (up to 41.5 T) down to 0.46 K, and the 1/9 plateau feature has been confirmed. Moreover, the temperature dependence of C_p/T in the vicinity of 1/9 plateau region can be fitted by a linear in T term which indicates the presence of a Dirac spectrum, together with a constant term, which indicates a finite density of states contributed by other spinon Fermi surfaces. Surprisingly, the constant term is highly anisotropic in the direction of the magnetic field. Additionally, we observe a double-peak feature near 30 T above the 1/9 plateau which is another hallmark of fermionic excitations in the specific heat. This combination of gapless behavior and the double-peak structure strongly suggests that the 1/9 plateau in YCOB is nontrivial and hosts fermionic quasiparticles.

DOI: 10.1103/PhysRevX.15.021076 Subject Areas: Condensed Matter Physics

I. INTRODUCTION

Quantum spin liquids (QSLs) have played an essential role in condensed matter physics since Anderson proposed the resonating-valence-bond model in 1973 [1]. The spin-1/2 kagome Heisenberg antiferromagnet (KHA) exhibits a high degree of geometric frustration and is one of the most promising candidates for hosting QSLs [2–4]. Theoretically, the presence of QSL on the KHA has been confirmed by density matrix renormalization group simulations [5], but its precise ground state remains an open question, with two main possibilities: the gapped Z_2 spin liquid [5–7] and the gapless U(1) Dirac spin liquid (DSL) [8–11]. Beyond the ground state at zero field, more exotic quantum entangled states can emerge under magnetic fields, such as the unconventional 1/9 magnetization plateau, which might be described by a topological Z_3 QSL [12] or a gapless valence-bond-crystal state [13], though its nature remains elusive. A recent projected Monte Carlo study supports a Z_3 spin liquid scenario with fermionic spinons [14].

Experimentally, the most extensively studied QSL candidate in the kagome system so far is herbertsmithite $[ZnCu_3(OH)_6Cl_2]$ [15,16]. The difficulty in determining its ground state arises from the partial substitution of the Zn^{2+} sites located between the two-dimensional (2D) kagome planes by Cu^{2+} ions, which causes the low-energy excitations to be dominated by these orphan spins [17–19]. Recently, the synthesis of the KHA $YCu_3(OH)_6Br_2[Br_x(OH)_{1-x}]$ (YCOB) has addressed the site mixing issue by introducing Y^{3+} ions which have a different ionic size than Cu^{2+} [20]. The first material, $YCu_3(OH)_6Cl_3$ had the ideal kagome structure [21] but was found to order at 15 K [22]. It has been known that the

*Contact author: luli@umich.edu

presence of a small Dzyaloshinskii-Moriya (DM) term leads to ordering [23], so this was not a complete surprise. The next development is the replacement of Cl by Br and a partial substitution of Br with OH as in YCOB, where no magnetic transition is found down to 50 mK [24]. However, it should be noted that the random substitution of Br by OH leads to a distribution in the exchange constant J [25]. Apparently, some kind of deviation from a uniform exchange constant is needed to overcome the DM term and suppress ordering. These developments make YCOB a compelling QSL candidate [20,24,25], even though disorder in the exchange coupling is now present.

YCOB received a lot of attention starting from the report that C_p/T has a linear T term [24,25] which develops a finite zero temperature extrapolation as a magnetic field is applied [24]. This was taken to be a signature of a Dirac spin liquid, where the low-energy excitations are fermionic spinons obeying a 2D Dirac spectrum. This material has been under intense study using a variety of techniques such as nuclear magnetic resonance [26,27], nuclear quadrupole resonance, and muon spin relaxation [28], neutron scattering [29], thermal conductivity [30], and magnetization [31], as well as detailed sample characterization under different alloying and growth conditions [32]. While some of these data support the Dirac spin liquid picture, the interpretation is not fully consistent. One point is that spin susceptibility measurements find that dM/dH goes to a constant at low temperatures, which is at variance with the prediction of linear T behavior based on the Dirac spinon model. Another puzzle is that thermal conductivity finds a very small enhancement in magnetic fields up to 6 T, which indicates that the spinon contribution is very small and the mean free path of the spinons, if they exist, is very short, perhaps due to disorder [30]. On the other hand, the sharpness of the neutron scattering peak structure [29] argues against strong disorder.

It should be added that, amid these uncertainties, what is clear is that YCOB at low magnetic fields is not described by the random singlet model, which has been successful in describing the low T, H behavior of a wide array of "spin liquid candidates" which do not order down to low temperature, including herbertsmithite [33,34]. In this picture, the exchange J between the orphan spins obeys a power law distribution $J^{-\nu}$. At a given temperature, a fraction $T^{1-\nu}$ of the spins are free, leading to the prediction that both C_p/T and dM/dH scale as $T^{-\nu}$, where ν is found empirically to be between 0.3 and 0.5. Note that, for this model to make sense, the distribution of J must be singular for small J and ν must be positive. The predicted behavior is very different from the behavior observed in C_p/T and dM/dH as discussed earlier [25].

Against this backdrop of uncertainties, we embarked on a study of YCOB under an intense magnetic field, with the hope that the strong Zeeman energy may bring new insight. Indeed, three independent groups discovered a magnetization plateau at $1/3$ and $1/9$ [35–37]. As mentioned earlier, the $1/9$ plateau was predicted by theory and can signal a nontrivial new state. Furthermore, high-resolution magnetic torque measurements found oscillations in the magnetization [35], reminiscent of quantum oscillations in metals. This is highly unexpected in a 3 eV band gap insulator. This observation was interpreted in terms of fermionic spins with a Dirac spectrum [35]. The novelty of these data and the lack of consensus on whether the $1/9$ plateau is gapped [37] or gapless [35] makes it imperative to study the $1/9$ plateau using other probes.

In this paper, we report the specific-heat (C_p) measurements on single crystals of YCOB under magnetic fields of up to $\mu_0 H = 41.5$ T, with temperatures down to $T = 0.46$ K. The $1/9$ plateau phase previously observed in magnetization is verified in the magnetic-field dependence of the specific heat. We find a finite value for C_p/T in the $T \to 0$ limit, which provides direct evidence that the system has gapless excitations. We also find a linear T term in C_p/T which is consistent with Dirac spinon contribution. More importantly, we constructed a Wilson ratio (W_D) by combining the magnetic susceptibility and specific-heat data at the $1/9$ plateau for Dirac fermions. The resulting value of $0.29 \le W_D \le 1.14$, which is close to unity, provides significant support for the existence of Dirac fermions within the $1/9$ plateau phase. Moreover, we observe a "double-peak" structure in C_p similar to what was seen in graphite and interpreted as coming from thermal broadening of a sharp fermionic state. This provides additional important evidence of the fermionic nature of the excitations. We emphasize that the main focus of this paper is on the nature of the $1/9$ plateau. We believe the quantum state that characterizes this plateau is distinct from the low-magnetic-field state. A peak in the specific heat which separates the onset of the $1/9$ plateau from the low-field regime supports this notion. From this point of view, the data reported in this paper do not shed additional light on the nature of the low-field state, and we do not discuss the low-field state further.

II. EXPERIMENT

For this study, single crystals of YCOB were grown using the hydrothermal method as reported previously [24]. The magnetization measurements on YCOB sample $M1$ were performed using a compensated coil spectrometer [38,39] in a 65 T pulsed field magnet at the National High Magnetic Field Laboratory (NHMFL), Los Alamos. The specific-heat measurements on YCOB sample $H1$ at high fields were carried out using a membrane-based nanocalorimeter [40] employing an ac steady-state method [41] in the 41.5 T cell 6 dc field magnet at NHMFL, Tallahassee. Unless otherwise specified, all specific-heat measurements were performed on YCOB sample $H1$. The specific-heat data presented for the YCOB $H1$ sample in the main text have been processed to subtract the contribution from the addenda. The addenda subtraction method is described in the Appendix. The specific-heat measurements on YCOB sample $H3$ at 0 T in the inset in Fig. 2 were conducted in a Quantum Design physical property measurement system (PPMS) using the He-3 option.

III. RESULTS

A. One-ninth plateau in magnetization and specific heat

The magnetic-field (H) dependence of magnetization M and the corresponding derivative $\chi_M \equiv \mathrm{d}M/\mathrm{d}H$ for $H \parallel c$ and $H \parallel ab$ at temperature $T = 0.6$ K are shown in Fig. 1(a). The experimental details and sample growth information are given in Sec. II. The plateau region can be characterized by the width of the valley in χ_M, which spans from 15.0 to 28.4 T when $H \parallel c$ and from 19.1 to 27.3 T when $H \parallel ab$. This observation is consistent with the results reported in Refs. [35–37]. The slightly larger 1/9 magnetization value when $H \parallel c$ can be understood by the anisotropy of the g factor [25]. To confirm the 1/9 plateau feature and shed light on this unconventional state, we conducted specific-heat measurements at high fields. The field dependence around the 1/9 plateau region is shown in Fig. 1(b) with applied field along $H \parallel c$ and $H \parallel ab$. The 1/9 plateau phase is visible as a dip in specific heat within the same field range. The similar behavior of the $\mathrm{d}M/\mathrm{d}H$ and C_p data in the 1/9 plateau phase is expected in the fermionic spinon picture, as both are directly related to the spinon density of states (DOS). We note that, in the region ($\mu_0 H > 10$ T, $T < 2$ K) which is our focus in this paper, specific-heat contributions from Schottky anomalies and phonons are negligible compared to the intrinsic C_p from the kagome plane, as discussed in the Appendix. Note that earlier heat capacity measurements [24,32,42] suggest traces of a nuclear Schottky anomaly for $\mu_0 H > 10$ T; this may reflect differences between earlier and later sample batches.

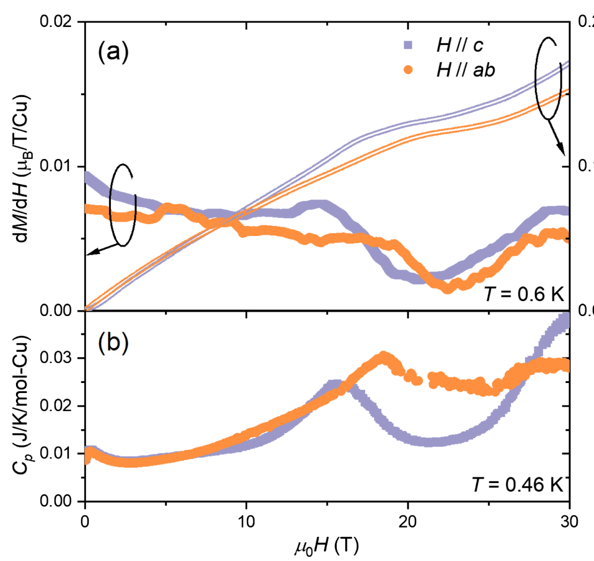

FIG. 1. Magnetic-field dependence of magnetization, the corresponding derivative, and specific heat around 1/9 plateau phase. (a) The thinner double lines represent the M versus H data measured at 0.6 K with applied field along the c (blue) and ab (orange) directions. The magnetic susceptibilities $\chi_M \equiv \mathrm{d}M/\mathrm{d}H$ are plotted as the thicker dots corresponding to the vertical scale on the left side. The 1/9 magnetization plateau is observed along the c axis between 15 and 28 T and in the ab plane between 20 and 27 T. (b) The field dependence of specific heat measured at 0.46 K with applied field along the c and ab directions. The clear valleys centered around $\mu_0 H_0 = 21$ T when $H \parallel c$ confirmed the 1/9 plateau in magnetization.

Zero-field specific-heat data up to 10 K are depicted in the inset in Fig. 2. The broad hump around 2.5 K is similar to what has been reported in Refs. [24,25,28,36]. As T approaches zero, C_p/T shows linear behavior with a vanishingly small intercept, as indicated by the black dashed linear fit. Our C_p data are in good agreement with the reports in Refs. [24,25].

B. Fermionic behavior at the center of the one-ninth plateau

To investigate the properties of the 1/9 plateau phase, the T dependence of C_p/T within the plateau regions below 5 K with field applied along the c axis and in the ab plane

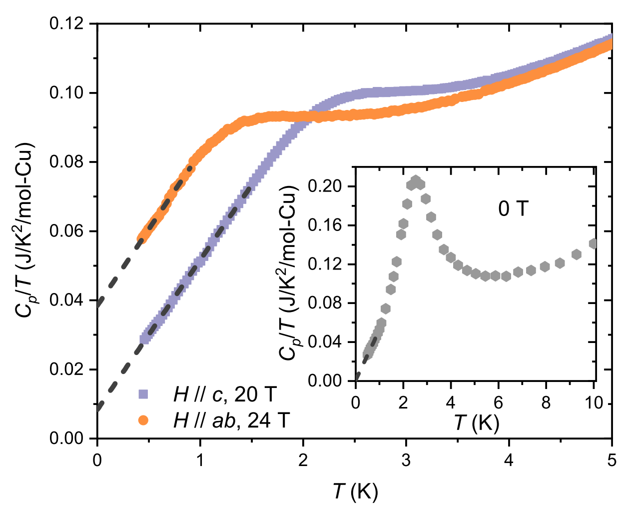

FIG. 2. Specific-heat data providing evidence for the gapless nature in the 1/9 plateau phase. The raw data of C_p/T versus T are presented down to 0.46 K with $\mu_0 H = 20$ T along the c axis (blue dots) and $\mu_0 H = 24$ T in the ab plane (orange dots). The field values are chosen to represent the middle of the plateau after taking into account the g-factor anisotropy. The black dashed lines are the linear fittings $C_p/T = \gamma + \beta T$. Note that, while the linear slopes are parallel, the finite intercept γ strongly depends on the field direction. The inset plot depicts the temperature dependence of specific heat of YCOB sample $H3$ at zero magnetic field, and the black dashed line is a linear fit with negligible intercept.

are plotted in Fig. 2. We notice that the broad hump shown at 0 T is significantly suppressed in the $1/9$ plateau region, and no phase transitions are detected at low T. This contrasts with the sharp peak feature in specific heat observed near the $1/3$ magnetization plateau region reported in some triangular lattices [43]. Moreover, as T approaches zero, C_p/T shows a linear T behavior with a finite intercept in both directions. The finite intercepts show that the $1/9$ plateau phase is gapless. The intercept shows a surprisingly large anisotropy when H is applied in different directions, as already clearly seen in Fig. 1(b). The data can be described by a linear fit:

$$C_p/T = \gamma + \beta T. \tag{1}$$

As shown by the black dashed lines in Fig. 2, it is clear that the linear slopes are almost parallel, while the intercept γ is different in the two directions. We obtained $\gamma_c = 8.0(5)$ mJ/K^2/mol-Cu, $\beta_c = 43.6(5)$ mJ/K^3/mol-Cu for $H \parallel c$ and $\gamma_{ab} = 38(1)$ mJ/K^2/mol-Cu, $\beta_{ab} = 44(1)$ mJ/K^3/mol-Cu for $H \parallel ab$. The fact that the β value is isotropic in the $1/9$ plateau phase, while γ is highly anisotropic, suggests that the γ and β terms may have different origins. Here, we remark that these data already answer the first important question posted earlier of whether the excitations are gapped or gapless in the $1/9$ plateau. The finite γ, whatever its origin, is direct evidence that the system is gapless. It is noteworthy that dM/dH also shows a finite intercept at low temperatures [35–37]. Despite this, Ref. [37] claims that the system is gapped. They base their argument on the existence of DM terms which break the conservation of total spins. Presumably they have in mind an analog of the Van Vleck term that gives a constant dM/dH even in an insulator with spin-orbit coupling. Our specific-heat data directly rule out this possibility.

Now, we first focus on the β term and return to discuss the γ term and its anisotropy later in the paper. In a 2D Dirac free fermion, we define the theoretical value $\tilde{\beta} = C_p/T^2 = 18 n_D \zeta(3)\pi k_B^3 A_s/(2\pi\hbar v_D)^2$, where n_D is the degeneracy of Dirac nodes, A_s is the area of the 2D system, and v_D is the Dirac velocity [8]. Using $\beta = 43.6$ mJ/K^3/mol-Cu, we can estimate $v_D/\sqrt{n_D}$ to be 1.65×10^3 m/s $= 10.9$ meV $\cdot$ Å. The same quantity was estimated from the approximately linear slope in dM/dH versus H in Ref. [35] to be $(g'/g) \times 4.9$ meV $\cdot$ Å, where g' is the effective g factor which describes the movement of the down-spin chemical potential in a magnetic field. In Ref. [35], g'/g was taken to be approximately 2, but there is considerable uncertainty. Given these uncertainties and the fact that there can be corrections to the free-fermion formulas due to interaction effects, the agreement is reasonable.

Yet another point of comparison is that the temperature dependence of dM/dH at the center of $1/9$ plateau was found to be a constant plus a linear T term $\beta_\chi T$ [35]. The theoretical expression for the linear T coefficient is given as $\tilde{\beta}_\chi = \ln(2)(g'/2)^2 \mu_B^2 n_D/\pi\hbar^2 v_D^2$. By fitting the data, a value for $v_D/\sqrt{n_D}$ was found to be 1.72×10^3 m/s by taking $g' = 2g$ [35]. Using the theoretical expression for the T^2 term in the specific heat given above, we can construct the analog of the Wilson ratio for Fermi liquid to Dirac fermions by comparing the ratio between the linear T term in dM/dH and C_p/T to that of free fermions, which we denote this as *Dirac Wilson ratio*:

$$W_D = \frac{\beta_\chi/\beta}{\tilde{\beta}_\chi/\tilde{\beta}}, \tag{2}$$

where again the β_χ is the T-linear coefficient of the magnetic susceptibility near $T = 0$, β is the T-quadratic coefficient of the specific heat near $T = 0$, and $\tilde{\beta}$ and $\tilde{\beta}_\chi$ are the theoretical expectations for the free Dirac fermions.

The advantage of the Dirac Wilson ratio is that parameters such as n_D and v_D are canceled. If the system is described by free Dirac fermions, the Wilson ratio $W_D = 1$. Because the temperature-dependent data for χ in the ab plane are not available in Ref. [35], we examine only the Dirac Wilson ratio along the c axis in the following part. Using the expressions given above, we find that $\tilde{\beta}_\chi/\tilde{\beta} = 0.13(g'/2)^2\mu_B^2/k_B^2$. From the data, we find $\beta_\chi = 0.63 \times 10^{-3}\mu_B$/T/K/Cu [35] and $\beta = 43.6$ mJ/K^3/mol-Cu, so that $\beta_\chi/\beta = 0.18\mu_B^2/k_B^2$. Hence, we find $W_D = 1.38(2/g')^2$. If we take the conventional g factor, $g' = g = 2.2$ [25], then $W_D = 1.14$, which is very close to unity. However, as we mentioned before, there could be a correction to g' near the Dirac node region, as derived in Ref. [35], where $g' \approx 2g$, resulting in $W_D = 0.29$. Given the uncertainty of the value of g', we consider g' to be within the range $2g \geq g' \geq g$. Consequently, W_D should fall within the range $0.29 \leq W_D \leq 1.14$.

In addition to the Dirac Wilson ratio, we can also estimate the conventional Wilson ratio for a spinon Fermi surface, given the presence of a finite γ in Fig. 2. The established Wilson ratio for a Fermi liquid is given by

$$R_W = \frac{\pi^2 k_B^2}{3(g'/2)^2\mu_B^2}\frac{\chi_0}{\gamma}, \tag{3}$$

where χ_0 is the magnetic susceptibility at zero temperature. From the data in Ref. [35], we obtain $\chi_0(20\ \mathrm{T}) = 1.8 \times 10^{-3}\mu_B$/T/Cu and $\gamma(20\ \mathrm{T}) = 8$ mJ/K^2/mol-Cu for a field along the c axis. Using these values, we estimate the Wilson ratio for a spinon Fermi surface as $R_W = 9.1(2/g')^2$. If we adopt the same range $2g \geq g' \geq g$, then the resulting range of R_W should be within $1.88 \leq R_W \leq 7.52$.

For the Fermi surface case, the conventional Wilson ratio is subject to corrections due to Landau Fermi liquid parameters in the presence of interaction [44]. These corrections could lead to an enhanced Wilson ratio, as observed in the heavy fermion metal CeFePO where $R_W = 5.5$ [45]. Given the strong correlations in YCOB, it is reasonable to expect a Wilson ratio greater than 1. Such correction does not exist for Dirac fermions, because the density of states vanishes at the chemical potential. Thus, the deviation of the Dirac Wilson ratio from unity can potentially be a difficulty for the Dirac spinon model. Here, we point to an interesting escape route. In the presence of n_D Dirac nodes, if n_D is large enough, the gauge field is deconfined and has a linear dispersion like a photon. In 2D, this gives a T^2 contribution to the specific heat which should be added to the fermion contribution. Therefore, the Dirac Wilson ratio being unity is just an upper bound. We consider the fact that the Dirac Wilson ratio is of the order of but less than unity to be a significant support for the Dirac fermion model.

In principle, the T^2 dependence in C_p can be due to some critical or Goldstone 2D bosonic mode with a linear dispersion. It should be noted that, in this scenario, dM/dH would generally not show a linear T dependence. It may be gapped or follow some other exponent. Therefore, one would need a separate explanation of why dM/dH is gapless and has a linear T dependence with a Dirac Wilson ratio close to unity.

C. Features of the specific-heat data over a broad range of magnetic field and temperature

In this section, we take a step back and provide a broader view of specific-heat data. We show the data taken over a wide range of magnetic field ($H \parallel c$ and $\parallel ab$) and temperature. First, consider Fig. 3(a). The 1/9 plateau is seen as a dip at $H = H_0 \approx 21$ T as marked by the dashed blue line. This dip gradually fills in with increasing T. For the lower field, there is a broad peak centered at $H_p \approx 16$ T, which moves to the lower field with increasing temperature, as marked by the dashed black line. In addition, there is another broad peak centered at $H^* \approx 29.5$ T. Interestingly, this peak splits as the temperature is raised, as marked by the dashed orange and red lines. The interpretation of this split peak is given later. Here, we mention that this peak is unrelated to the quantum oscillations seen by the torque measurement for field above 20 T [35]. There the effect is very small, of the order of a few percent, which is beyond the resolution of the specific-heat measurement. Also, the peaks in the magnetization oscillations are not temperature dependent and show very different dependence on field orientation compared with H^*.

Returning to the peak near H_p, it is marked by a dashed black line as T is increased. Later, it is shown in Fig. 5 that the position of the peak shifts as T^2. We note that 16 T is close to the onset of the 1/9 plateau in the magnetization as shown in Fig. 1(a). A similar peak is seen for $H \parallel ab$ shown in Fig. 3(b) which has a similar T^2 dependence in its

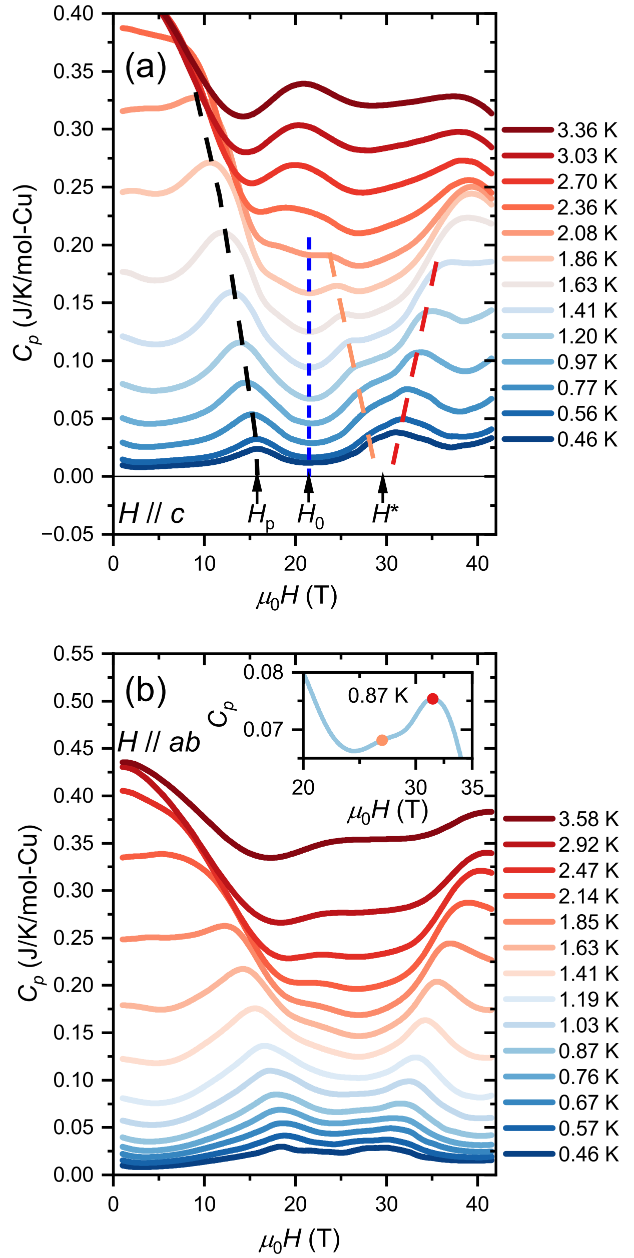

FIG. 3. Raw data of C_p. (a) The field dependence of C_p at different T with H applied along the c direction. The black dashed line traces the location of a peak located at $\mu_0 H_p = 16$ T at low T and its evolution with increasing T, the blue dashed line marks the middle of 1/9 plateau region $\mu_0 H_0 = 21$ T, and the orange and red dashed lines are guides for tracking the shift of two split peaks at $\mu_0 H^* = 29.5$ T. (b) The field dependence of C_p at different T with H applied in the ab plane. The inset provides an enlarged view of the C_p data when $T = 0.87$ K, highlighting the presence of split peaks around 30 T for $H \parallel ab$ case, which are marked by orange and red dots.

position, except that now it starts at approximately 19 T, which is where the plateau begins for this field orientation. We are, thus, motivated to interpret this peak as marking the onset of the 1/9 plateau phase as a quantum phase

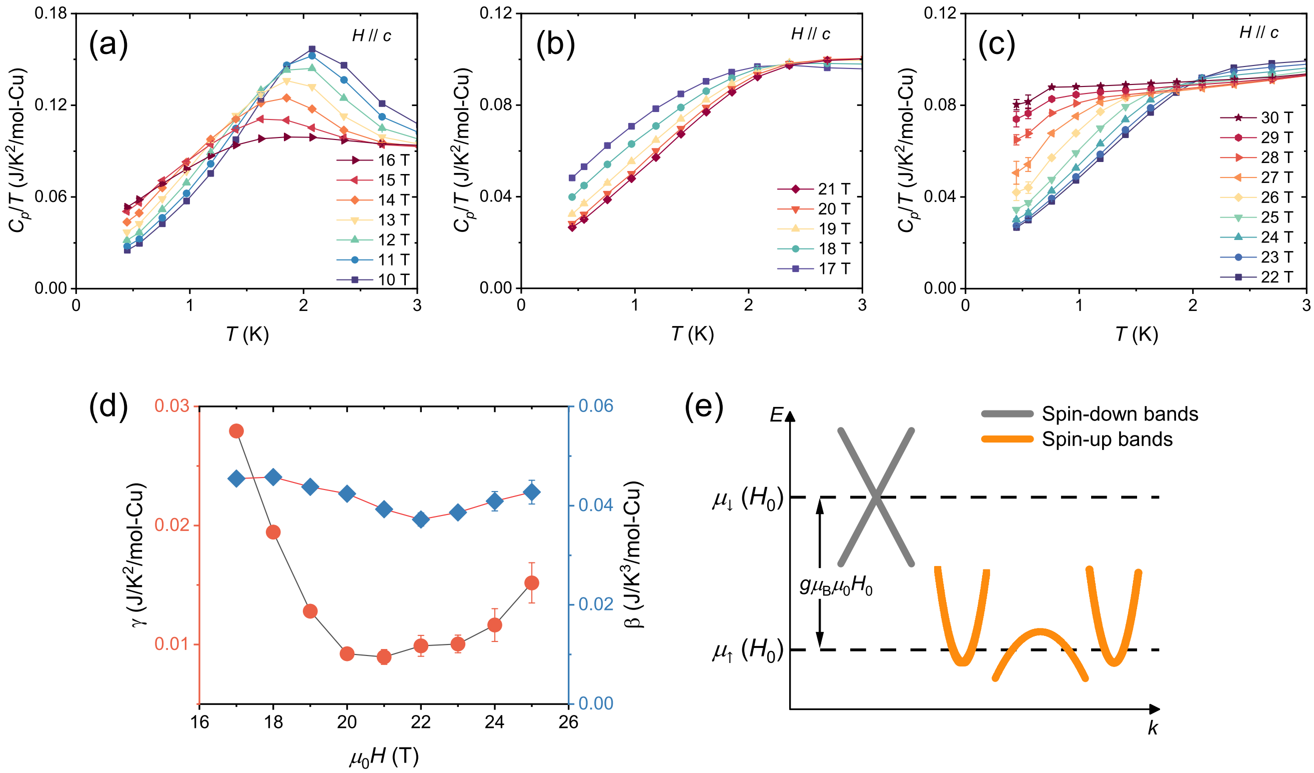

FIG. 4. Field evolution of fermionic behavior in the vicinity of $1/9$ plateau region. (a)–(c) T dependence of C_p/T for different fields with $H \parallel c$. Data are cut from Fig. 3 at fixed fields. (d) The field dependence of values of γ (red dots) and β (blue dots) from 17 to 25 T, obtained from linear fits of C_p/T versus T data in (a)–(c) via Eq. (1) in the temperature range $0.46 \le T \le 0.77$ K. (e) A sketch of the spinon band structure around H_0, which is based on a 2D Dirac spinon (gray bands) centered at the spin-down chemical potential $\mu_\downarrow(H_0) = E_0$ combined with a set of particlelike and holelike bands (orange bands) that cross the spin-up chemical potential $\mu_\uparrow(H_0)$. The spinon model is described in Sec. III D.

transition. Generally speaking, this transition may be broadened to a crossover by disorder in the exchange J, and no true singularity is observed. The T^2 dependence may indicate a crossover temperature that scales as $|H - H_p|^{0.5}$. However, since the nature of the respective quantum phases is not known, we do not pursue this point further. We point out only that if this peak is indeed due to critical fluctuations of some soft mode, it is bosonic in nature and should not be interpreted in terms of fermionic excitations. In fact, we see that its tail overlaps with fermioniclike excitations in the plateau phase and complicates its analysis.

To gain further insight, the low-temperature dependence of C_p/T over separate ranges of magnetic fields ($H \parallel c$) is plotted in Figs. 4(a)–4(c). The data were taken from the vertical line cut in Fig. 3(a) at a fixed field. A broad hump around 2 K, as shown in Fig. 4(a) at 10 T, closely resembles the hump observed at zero field in the inset in Fig. 2. However, this hump rapidly diminishes as the field approaches the $1/9$ plateau phase and is absent at 16 T. It is interesting to compare our 10 T data with the 9 T data available in the literature. While they all show a linear T dependence, our data show a very small intercept γ which disagrees with a γ which was originally reported to be linear in H [24]. However, a recent study [32] found that this γ depends on sample preparation, and our data are very similar to that shown in Fig. 6(f) in Ref. [32], on a sample that is prepared in a similar way. We do not dwell further on this point, because our present study focuses on the high field regime near the $1/9$ plateau, which may be separated from the more sample-sensitive low-field regime by a quantum critical point, as mentioned earlier.

To study the field evolution of the γ and β coefficients inside the $1/9$ plateau phase, we performed linear fits of the temperature dependence of the specific-heat data based on Eq. (1) in the range $0.46 \le T \le 0.77$ K for fields between [17, 25] T. The field dependence of γ and β is shown in Fig. 4(d). We find that β is almost constant over this field range, while γ is constant between 20 and 23 T but increases for lower and higher fields. The low-field increase is likely from the tail of the peak at H_p. As mentioned earlier, the peak near 16 T may be a bosonic soft mode marking an underlying quantum critical point. In that case, the rise in γ for a field below 19 T, which includes the contribution from the peak at H_p, should not be confused with the γ that originates from a finite DOS in a fermion model. Similarly, it is clear from Fig. 3(a) that the data for $H > 24$ T are picking up contributions from the split peak, especially as the temperature is raised. We see from Fig. 4(c) that the linear T regime shrinks as H exceeds 25 T. This is why we began our analysis in Fig. 2 by focusing on the field along c at 20 T. From the discussion in this section, we believe the fit to Eq. (1) is reliable for the field range between approximately 20–23 T but not outside this range. We, therefore, conclude that, near the plateau minimum, the specific heat is consistent with Dirac spinons located at H_0, plus some other contributions that give the finite γ value.

D. Dirac spinon model

In this section, we show that the 2D phenomenological model introduced in Ref. [35] to explain the $1/9$ magnetization plateau and oscillations is consistent with our specific-heat data. In this picture, in the middle of the plateau at field H_0, the spin-down chemical potential $\mu_\downarrow$ crosses a 2D Dirac spinon band, while the spin-up chemical potential $\mu_\uparrow$ crosses electronlike and holelike bands, forming a spinon semimetal with total density zero. This is shown in Fig. 4(e). It is natural to interpret the linear term in C_p/T as originating from the linear DOS of the Dirac spectrum. On the other hand, the finite $\gamma_c = 8\ \mathrm{mJ/K^2/mol\text{-}Cu}$ around $\mu_0 H_0 = 21$ T could be attributed to the bands at $\mu_\uparrow$. The reason for the large anisotropy in γ is not well understood, but we return to discuss this later. Putting this question aside, in the next section, we show that the double-peak feature H^* can also be accommodated in the fermionic spinon model by including a saddle point in the spinon DOS.

E. Double-peak structure

In this section, we discuss the origin of the double-peak structure. We already mentioned the three kinds of peak or valley features visible in Fig. 3. We tracked the locations of these peaks and valleys and plotted them in Fig. 5. The first feature is the crossover peak at $\mu_0 H_p \approx 16$ T between the zero-field ground state and the $1/9$ plateau phase. The T evolution of the peak location is plotted in Fig. 5 as black squares, which are well fitted by a power law $\mu_0 H - \mu_0 H_p \propto T^2$, where $\mu_0 H_p = 16.13(7)$ T. As mentioned earlier, this interesting quadratic behavior may be related to quantum criticality separating the low-field state from the plateau state. Next is the $1/9$ plateau valley centered at $\mu_0 H_0 \sim 21$ T, whose location has almost no T dependence as indicated in Fig. 5 by blue stars. The next feature is a broad peak seen at $\mu_0 H^* \sim 29.5$ T in Fig. 3(a). At first glance, this appears to be a symmetric counterpart of the peak at H_p. However, the T dependence of the peak at H^* indicates that it may have a different origin. As T increases, this peak splits into two peaks as tracked by the orange and red dashed lines in Fig. 3(a). We note that for $H \parallel ab$ a similar peak can be seen at $H \approx 30$ T in Fig. 3(b). A more subtle splitting can also be seen in the inset in Fig. 3(b) at 0.87 K. At higher T, the split peak is too broad

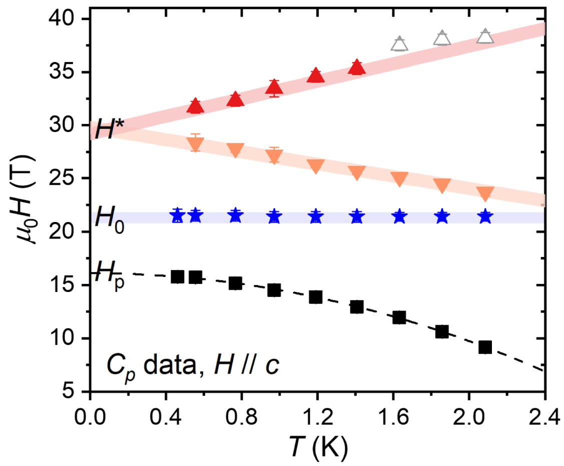

FIG. 5. Phase diagram of YCOB characterized by C_p. The data points are the peak or valley locations taken from Fig. 3(a) with the corresponding color codes. Solid lines are linear, while the dashed line is quadratic in T.

to be resolved. On the other hand, the peak at $H \approx 19$ T shifts with temperature in the same way as the H_p peak for $H \parallel c$. Since both peaks align with the onset of the $1/9$ magnetization plateau shown in Fig. 1(a), we interpret them in a similar manner as marking the onset of a new quantum state.

Taking the derivative of C_p makes the peak-splitting effect sharper, as displayed in Fig. 6(a), also as orange and red lines. For reasons mentioned earlier in Sec. III C, the features above 25 T at low temperatures are not related to the magnetization oscillations observed in Ref. [35]. Here, we present an explanation in terms of the double-peak splitting of a Van Hove singularity. The peak positions around H'^* in Fig. 6(a) are plotted in Fig. 6(b). These can be described by two linear fits with the intercept falling in the same field range. We note that the red hollow data points in Figs. 5 and 6(b) are excluded from the fitting, because they may be interfered with by another peak in higher field ranges (>40 T). In Fig. 6(b), the linear fits are carried out using the expression $\mu_0 H = \mu_0 H'^* + k' T$. The fitting results are $\mu_0 H'^* = 28.6(3)$ T, $k' = -2.9(2)$ T/K for orange data points and $\mu_0 H'^* = 28.7(5)$ T, $k' = 3.1(4)$ T/K for red data points. The overlapping intercepts and linear T dependence of the peak locations are reminiscent of the double-peak structure observed in the specific heat due to a narrow peak in the fermionic DOS [46]. To provide an explanation of the double-peak structure for fermionic excitations, we begin with the expression for the specific heat:

$$C_p(\mu, T) = \frac{\partial}{\partial T} \int D_D(E) \cdot (E - \mu) \cdot f_{\mathrm{FD}}(E - \mu) \mathrm{d}E, \qquad (4)$$

where $f_{\mathrm{FD}}(E-\mu) = 1/[\exp(E-\mu)/k_B T + 1]$ is the Fermi-Dirac distribution function.

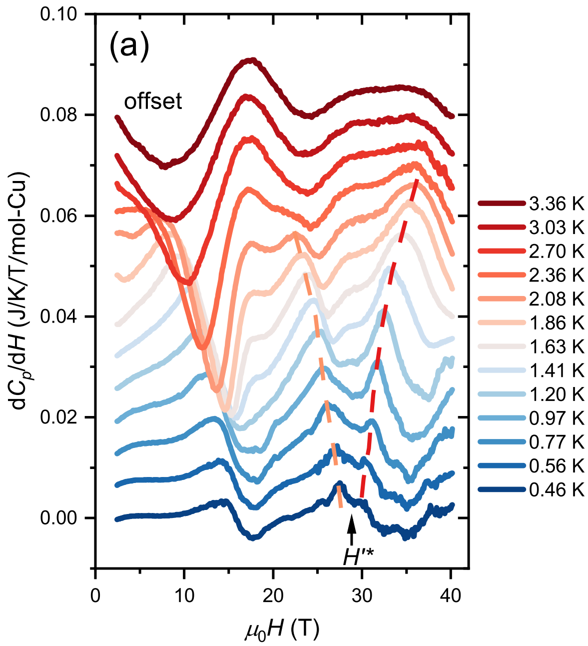

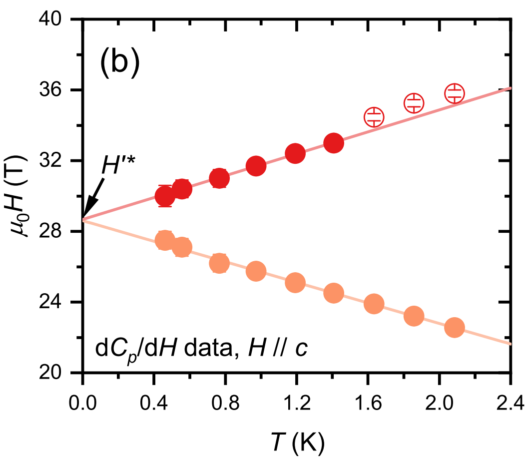

FIG. 6. Double-peak structure in the derivative of the specific heat. (a) Field dependence of the derivative of the specific heat $\mathrm{d}C_p/\mathrm{d}H$ at different T with a constant offset 7 mJ/K/T/mol-Cu for clarity. H'^* indicates the peak-splitting field in $\mathrm{d}C_p/\mathrm{d}H$ at 0 K. (b) The orange and red circles are field locations of two peaks shown by the orange and red dashed lines in (b). The orange and red lines in (b) are two linear fits for the corresponding data points, while the hollow red circles are excluded from the fits.

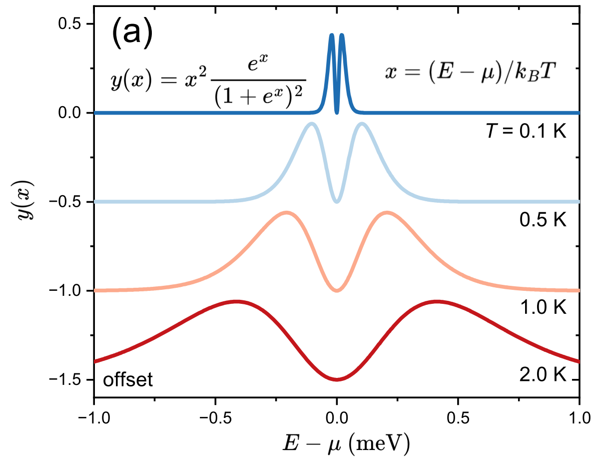

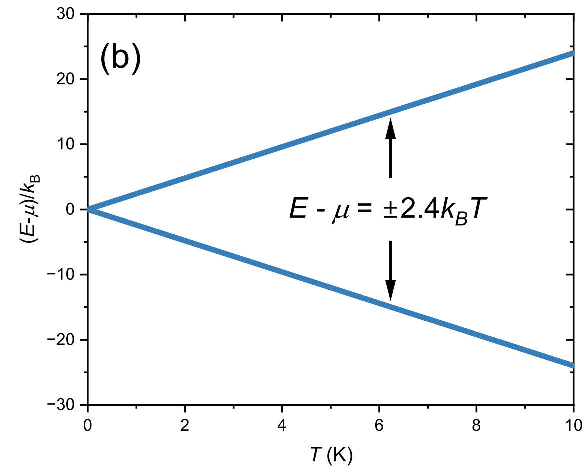

FIG. 7. The origin of double-peak structure. (a) The temperature evolution of $y(x) = x^2 \exp(x)/[1+\exp(x)]^2$, where $x = (E-\mu)/k_BT$ and μ is the chemical potential. (b) The temperature dependence of the locations of two peaks in (a), which can be described by the linear equations $E-\mu = \pm 2.4 k_BT$.

We set $(E-\mu)/k_BT = x$ and rewrite Eq. (4) as

$$C_p(\mu, T) = k_B^2 T \int D(\mu + x) x^2 \frac{e^x}{(e^x+1)^2} \mathrm{d}x. \qquad (5)$$

Reference [46] called attention to the double-peak feature in the function $y(x) = x^2(\exp(x)/[1+\exp(x)]^2)$, which is plotted in Figs. 7(a) and 8(c). The specific heat is a convolution of the DOS with the function $y(x)$. Therefore, a narrow peak in the fermionic DOS D will produce a linear-in-T splitting in C_p/T as T exceeds the peak width, generating the so-called "double-peak" structure via Eq. (5). The T dependence of the double-peak locations is shown in Fig. 7(b), which is very similar to what is observed in Fig. 6(b). By setting the energy scale to be $E = sg\mu_B\mu_0H$ in Fig. 7(b), we can use the slope of the fits obtained from Fig. 6(b) to estimate the g factor. For H near 30 T, we find the g factor along the c axis to be 2.3(3) or 2.4(2), based on the slope of orange and red linear fits (k') obtained from Fig. 6(b), respectively. These values are consistent with the experimental value $g = 2.19$ when $H \parallel c$ as reported in Ref. [25]. This remarkable observation provides strong support for the fermionic nature of the excitation. In the fermionic spinon picture, a possible origin of the narrow peak is that it could be due to a Van Hove singularity away from the Fermi level in one of the spinon bands. The double-peak structure in specific heat has been studied in the graphite, due to the Landau quantization [46], as well as in the Kondo metal $CeRu_2Si_2$ [47] and the Kondo insulator YbB_{12} [48], where it arises from the singularity in the DOS at a Lifshitz transition. This distinctive feature in specific heat provides a powerful tool for distinguishing fermionic excitations from magnetic transitions. To our knowledge, this is the first observation of a double-peak structure in a 3-eV band gap insulator, providing strong evidence for the charge-neutral fermionic nature of excitations in YCOB above the 1/9 plateau.

F. Dirac spinon model simulation

In Sec. III D, we introduced a Dirac spinon model with a sketched band structure, which is valid near H_0. Building on this model and motivated by the observation of the double-peak structure, we attempt to extend our spinon model to field H^* by proposing a simplified DOS for the spin-down bands, which incorporates a Dirac node at H_0 and a Van Hove singularity at H^*. The parabolic bands of spin up providing a constant $\gamma_c = 8\ \mathrm{mJ/K^2/mol\text{-}Cu}$ in Fig. 4(e) are still valid and are ignored in the following simulation.

The DOS used in our simulation is adapted from the DOS of graphene [49], which features a Dirac node at $E = 0$ and a Van Hove singularity at $E = t$, where t is the nearest-neighbor hopping energy. Here, we assume the spinon band structure of down spin in YCOB is given by

$$E_\downarrow(\mathbf{k}) = \mu_\downarrow(H_0) + E_g(\mathbf{k}), \tag{6}$$

where $E_g(\mathbf{k})$ is [49]

$$E_g(\mathbf{k}) = \pm t\sqrt{3 + 2\cos(\sqrt{3}k_y a) + 4\cos\left(\frac{\sqrt{3}}{2}k_y a\right)\cos\left(\frac{3}{2}k_x a\right)}. \tag{7}$$

Here, a is the lattice parameter, and t is determined by the energy level of the Van Hove singularity at H^*. By setting $t = 0.54$ meV, $\mu_\downarrow(H_0) = \frac{1}{2}g\mu_B\mu_0 H_0$, and $g = 2.2$, the resulting DOS for $E_\downarrow > \mu_\downarrow(H_0)$ part, derived from Eq. (6), is depicted as the blue area in Figs. 8(c)–8(e). Meanwhile, the function $y(x)$ as we defined before, centered at the chemical potential, is shown as the red curve. The heat capacity C is then calculated by the convolution of the DOS with $y(x)$ using Eq. (5). The calculated C is illustrated in Fig. 8(a). At $H = H_0$, corresponding to Fig. 8(c), the spin-down chemical potential $\mu_\downarrow(H_0)$ crosses the Dirac node, resulting in a minimum value of C, as indicated by the valley at H_0 in Fig. 8(a) at low temperatures. The symbols H^*, H_L^*, and H_R^* denote the field location of the Van Hove singularity at 0 K and the left and right peaks after splitting at finite temperatures, respectively. In Figs. 8(d) and 8(e), as the field increases to H_L^* and H_R^*, the integration in Eq. (5) yields two local maxima, leading to the double-peak structure observed around H^* in Fig. 8(a) at low temperatures.

To compare the simulation with experiments, the locations of the double peak in both experimental and simulated results, taken from Figs. 3 and 8(a), are plotted in Fig. 8(b). The temperature evolution of the field location for the left (H_L^*) and right (H_R^*) peaks shows good agreement, providing support for the presence of a Van Hove singularity in the fermionic DOS. Notably, the slope of H_L^* and H_R^* differ, which arises from the asymmetric shape of DOS near the singularity. This effect has been discussed in detail in Ref. [46]. We emphasize that the exact shape of DOS for the spin-down bands remains unknown and may be more complex than the simplified model we propose. Furthermore, the model is not applicable to the peak at H_p at the onset of the 1/9 plateau, shown in Fig. 3, which we have earlier ascribed to bosonic excitations possibly associated with a quantum critical point. The γ term and its anisotropy also require a separate discussion, which we present in the next section.

Using the proposed simplified DOS [blue curves in Figs. 8(c)–8(e)], we can examine the relationship between the 1/9 plateau phase and the double-peak structure. The 1/9 plateau corresponds to the linear DOS region which is the signature of Dirac spinons extending up to around 28 T (1.35 meV). The double-peak structure originating from the Van Hove singularity in DOS is centered around 29.5 T (1.88 meV). Thus, both the 1/9 plateau and the double-peak feature arise from the spinon band structure, with the double peak signaling a deviation from the Dirac band dispersion.

G. Origin of the γ term and its anisotropy in the one-ninth plateau

We begin by pointing out that the existence of a γ term in the specific heat in a spin system is highly unusual. A well-studied example is the two-level systems in structurally disordered insulators or spin-glass-like systems with competing interactions. Compared with our measurements, the γ terms are usually very small, because the number of two-level sites with small energy differences is rare. On the other hand, if the specific heat is dominated by a bosonic mode, the mode must have a k^2 2D dispersion as in a ferromagnet. This seems unlikely to be the case in YCOB. On the other hand, in the spinon model, what is needed is a spinon Fermi surface and a linear T term has been found in the organic materials κ-$(\mathrm{BEDT\text{-}TTF})_2\mathrm{Cu}_2(\mathrm{CN})_3$ [50] and $\mathrm{EtMe_3Sb[Pd(dmit)_2]_2}$ [51] and given this interpretation.

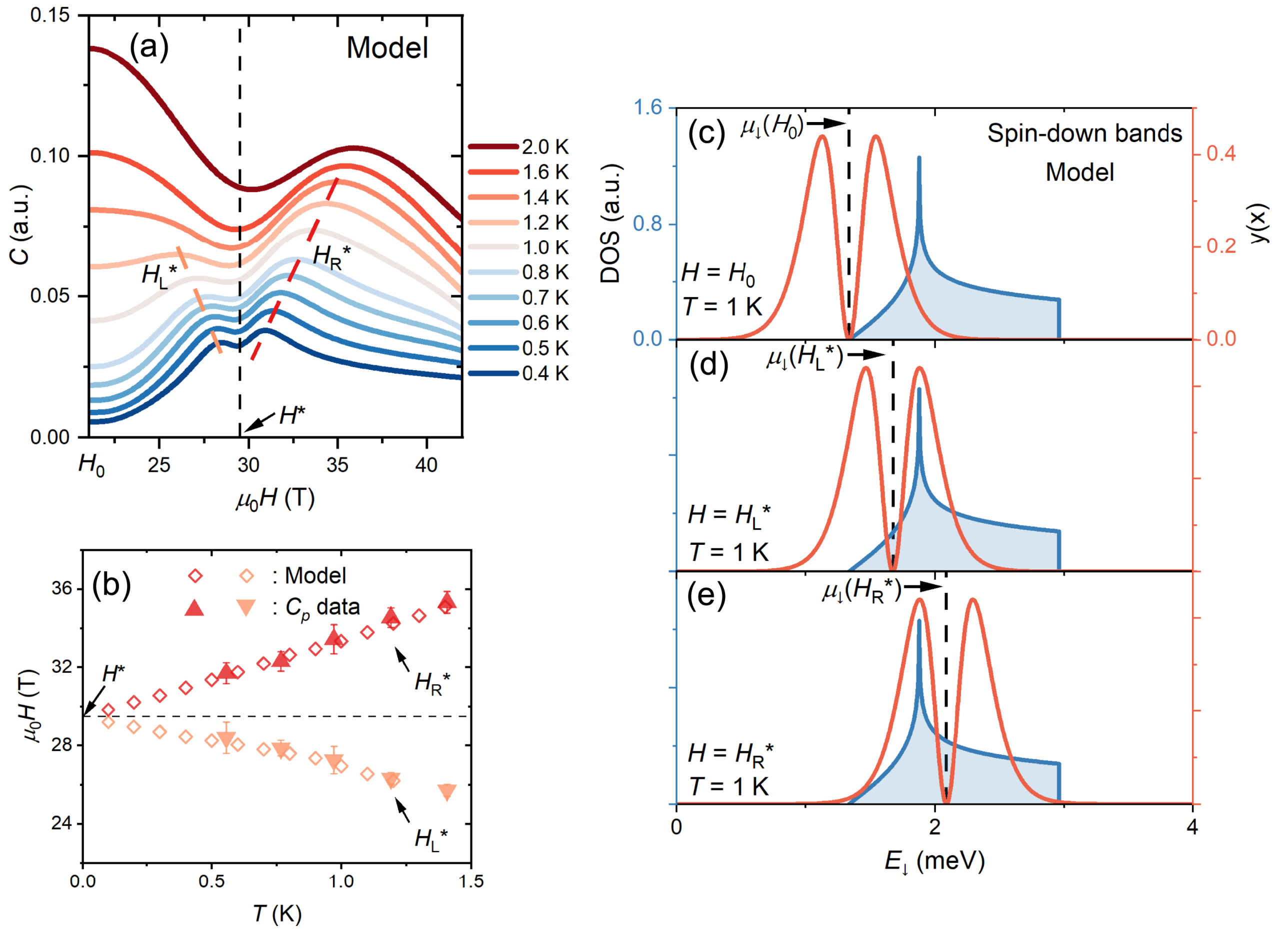

FIG. 8. Double-peak structure simulation. (a) The simulated field dependence of heat capacity C under different temperatures for spin-down bands based on the DOS shown in (c). H^* marks the peak location at 0 K before splitting. H_L^* and H_R^* represent field locations of the left and right branches, respectively, of the peak after splitting. (b) The red and orange diamonds represent T dependence of simulated values of H_L^* and H_R^*, respectively, while the red and orange triangles are the experiment data taken from Fig. 3(a). (c)–(e) The blue area denotes the DOS of the spin-down bands model given by Eq. (6). The main feature is the Dirac node when $\mu_\downarrow(H) = \mu_\downarrow(H_0)$ and the singularity when $\mu_\downarrow(H) = \mu_\downarrow(H^*)$. The red curve is the function $y(x)$ corresponding to the vertical scale on the left side.

However, the strong anisotropy observed in the experiment presented here poses a challenge to any model. We do not claim to have a definite solution, but we can offer some proposed directions.

Recall that, in the spinon model, at the middle of the plateau at $H = H_0$ the spin-down chemical potential $\mu_\downarrow$ crosses a Dirac spinon band, while the spin-up chemical potential $\mu_\uparrow$ crosses particlelike and holelike bands, forming a spinon semimetal. This is shown in Fig. 4(e). This will give a γ term in the specific heat. The question is why γ should depend so strongly on field orientation. On general grounds, we need spin-orbit coupling to break the rotational symmetry in spin space, and, in this material, there is a significant DM term, which is estimated to be about 15% of the exchange term in magnitude. In the spinon picture, the spinon dispersion can be affected by the DM term and becomes dependent on the field orientation. The DOS for the up-spin spinon depends sensitively on the band overlap, which gives rise to the particlelike and holelike Fermi surfaces shown in Fig. 4(e). This can be affected significantly by the DM term.

In this connection, it is interesting to note that the double peak feature at H^* shown in Figs. 3(a) and 3(b) remains at approximately 30 T for both $H \parallel ab$ and $\parallel c$. This is not what one would expect based on a spinon model with a dispersion that is isotropic. In that case, one expects both H_0 and H^* to shift proportional to the anisotropic g factor. In other words, the saddle-point-induced peak is expected to be at approximately 34 T. The fact that it does not shift implies that the band structure has to be anisotropic, so that the location of the saddle point relative to the Dirac crossing as shown in Figs. 8(c)–8(e) has changed with field orientation. As pointed out earlier, this is possible in the presence of the DM term. Interestingly, the shift of this relative position presents a possible explanation of the anisotropy of γ. For $H \parallel ab$, the double peak is only 6 T away from H_0, and its tail can add to the γ term, just as it affected the γ term beginning at approximately 24 T for

$H \parallel c$. From this point of view, the large γ for $H \parallel ab$ seen in Fig. 2 is a contribution from the tail of H^*.

Yet another possible origin of anisotropy is the gauge magnetic field, whose presence is needed to explain the quantum oscillations reported in Ref. [35]. The origin of the gauge magnetic field was proposed to be related to the DM term [52]. The gauge magnetic field will affect the spinon only when the applied magnetic field is along c. Thus, it is possible that the gauge magnetic field suppresses the DOS when H is applied along c by opening a gap. Our attempt at modeling this has not been entirely satisfactory, because it required additional assumptions and parameters and will not be reported here.

Our conclusion is that the anisotropy in γ is likely related to the DM term, which can lead to a spinon dispersion that depends on the direction of the magnetic field. The idea remains preliminary and further theoretical and experimental work is needed for further clarification.

IV. DISCUSSION

Finally, we compare our observations with specific-heat results in other QSL candidates. A finite γ value has been reported in different frustrated systems. Notably, the famous organic materials κ-$(\mathrm{BEDT\text{-}TTF})_2\mathrm{Cu}_2(\mathrm{CN})_3$ [50] and $\mathrm{EtMe_3Sb[Pd(dmit)_2]_2}$ [51] provided early evidence of spinon Fermi surface ground states. In another KHA material, herbertsmithite, a C_p/T which can be extrapolated to a γ value of 50 $\mathrm{mJ/K^2/mol}$ has also been observed in high magnetic field up to 34 T to suppress the local moment contributions, but no 1/9 magnetization plateau has been reported so far, and the field dependence of the specific heat at high fields is featureless [53,54]. In our case, the 1/9 plateau phase exhibits specific-heat characteristics that are entirely different from those of the conventional 1/3 plateau previously reported in other systems. For instance, the sharp λ-like peak feature in the T dependence of C_p around the gapped 1/3 plateau phase boundary in some triangular lattices, like $\mathrm{Cs_2CuCl_4}$ [55] and $\mathrm{Na_2BaCo(PO_4)_2}$ [43], is a signature of the transition into magnetically ordered states. In contrast, no sharp peak has been observed in the T dependence of C_p down to 0.46 K within the gapless 1/9 plateau phase as shown in Fig. 2. This difference strongly suggests that the 1/9 plateau phase could be an exotic spin-liquid plateau induced by the magnetic field [12].

V. CONCLUSIONS

In summary, we observed the unconventional 1/9 plateau in both the magnetization and specific heat in YCOB. The temperature dependence of the specific heat provides evidence that the 1/9 plateau is gapless with a finite DOS. Further field-dependent analysis indicates there could be a DSL in the 1/9 plateau phase centered at 21 T. The observed near-unity Dirac Wilson ratio provides direct thermodynamic proof of charge-neutral Dirac fermions in YCOB. Moreover, a Van Hove singularity at around 30 T can explain the double-peak structure observed at 30 T, thereby providing strong evidence for the fermionic nature of the excitation. The strong anisotropy of the γ term is a surprising feature that shows that spin-orbit coupling effects may be at play. Our results provide direct low-energy excitation information to understand the 1/9 plateau phase, providing evidence for an exotic DSL state associated with this plateau. These discoveries constitute a significant step in the search for QSL and the study of quantum entangled states.

ACKNOWLEDGMENTS

The work at the University of Michigan is primarily supported by the National Science Foundation under Grant No. DMR-2317618 (thermodynamic measurements) to K.-W. C., D. Z., G. Z., A. C., Y. Z., K. J., and L. L. The magnetization measurements at the University of Michigan are supported by the Department of Energy under Grant No. DE-SC0020184. A portion of this work was performed at the National High Magnetic Field Laboratory (NHMFL), which is supported by National Science Foundation Cooperative Agreements No. DMR-1644779 and No. DMR-2128556 and the Department of Energy (DOE). J. S. acknowledges support from the DOE BES program "Science at 100 T," which permitted the design and construction of much of the specialized equipment used in the high-field studies. The work at IOP China is supported for the crystal growth, by the National Key Research and Development Program of China (Grants No. 2022YFA1403400 and No. 2021YFA1400401), the K. C. Wong Education Foundation (Grant No. GJTD-2020-01), and the Strategic Priority Research Program (B) of the Chinese Academy of Sciences (Grant No. XDB33000000). The experiment in NHMFL is funded in part by a QuantEmX grant from ICAM and the Gordon and Betty Moore Foundation through Grant No. GBMF5305 to K.-W. C., D. Z., G. Z., A. C., Y. Z., and K. J. P. L. acknowledges the support by DOE office of Basic Sciences Grant No. DE-FG02-03ER46076 (theory).

APPENDIX: SPECIFIC HEAT DUE TO ADDENDA, SCHOTTKY, AND PHONON CONTRIBUTIONS

As mentioned in Sec. II, the specific heat of the YCOB $H1$ sample was measured by a membrane-based nanocalorimeter, which includes contributions from both the setup, referred to as the addenda, and the sample. The specific-heat contribution from the addenda is unavoidable and must be accounted for in the analysis. Here, we evaluate the specific heat from the addenda.

The specific-heat measurements of the addenda were conducted using the same membrane-based nanocalorimeter before loading the sample in 16T-SCMX at NHMFL.

The temperature dependence of the total specific heat measured with the YCOB $H1$ sample and without the sample (addenda) is shown in Fig. 9(a). From the inset, it can be observed that the specific heat of the addenda saturates at 12 T for low temperatures (below 1.5 K). This saturation at higher fields is likely attributed to the suppression of the Schottky anomaly, as discussed later. The field dependence of C_p from addenda at 0.46 K is given in Fig. 9(b), alongside the total C_p from the YCOB sample for comparison. The 0 T peak in the C_p of addenda is consistent with the Schottky anomaly, which explains the peak at 0.5 T in the YCOB sample data. It should be noted that the peak caused by the Schottky anomaly in the C_p of addenda appears incomplete due to a lack of data points.

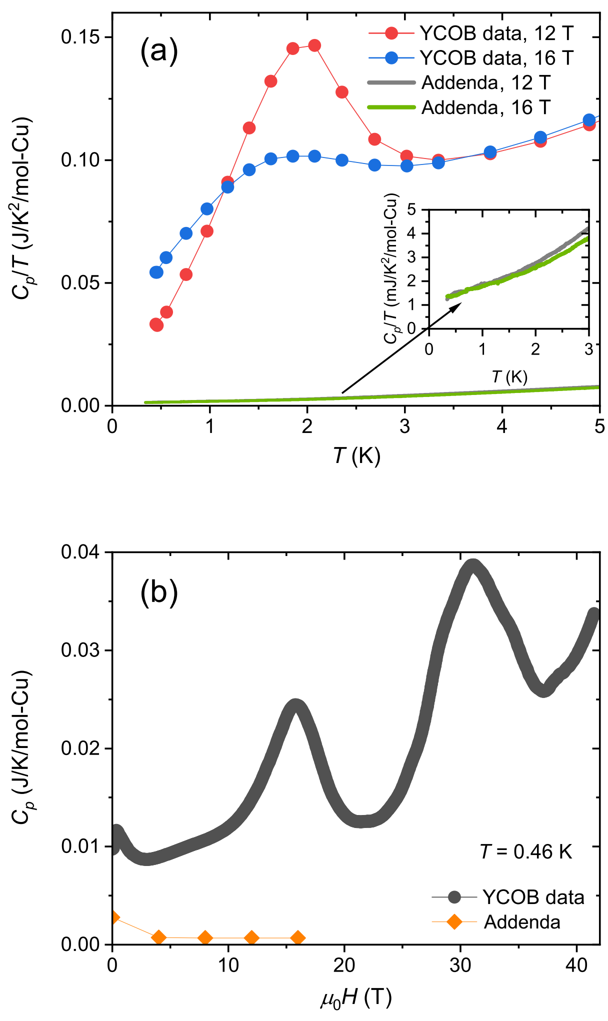

FIG. 9. Specific heat from addenda. (a) The temperature dependence of the total specific heat measured with the YCOB $H1$ sample (red and blue dots) and without the sample (addenda, gray and green curves, under magnetic fields of 12 and 16 T). An enlarged view of the addenda data is provided in the inset for clarity. (b) The field dependence of the total specific heat measured with the YCOB $H1$ sample (black dots) and without the sample (addenda, orange diamonds) at 0.46 K.

From the comparison, it is evident that the addenda contributes a small and nearly constant fraction (less than 5%) to the total specific heat when the field exceeds 10 T at fixed low temperatures. Since the low-field data for the YCOB sample include the Schottky anomaly from the addenda, this study focuses exclusively on the analysis above 10 T. We emphasize that *all* the data presented in the main text are derived by subtracting the addenda data at 16 T, shown in Fig. 9(a) as the green curve, from the total specific heat, to isolate the pure response from the YCOB sample.

To further analyze the specific heat from YCOB, we used the following expression:

$$C_p = C_{\mathrm{sc}} + C_{\mathrm{ph}} + C_{\mathrm{ka}}, \tag{A1}$$

where C_{sc} is the Schottky-like contribution arising from the localized excitations, which likely originates from the addenda, C_{ph} is the conventional phonon contribution, and C_{ka} is the specific heat originating from the kagome plane. As shown in Fig. 1(b) in the main text, a Schottky-like anomaly was observed at a low-field range (< 0.3 T) in both directions, which can be fitted by a two-level Schottky model:

$$C_{\mathrm{sc}} = f\frac{N_A k_B \Delta^2 e^{\Delta/T}}{T^2(1+e^{\Delta/T})^2}, \tag{A2}$$

where f is the fraction of orphan spins, Δ is the energy gap following $\Delta = g\mu_B\mu_0 H/k_B + \Delta_0$ with a field-independent gap Δ_0. The fitted result is shown in Fig. 10(a) using parameters $f = 0.087\%$, $g = 2$, and $\Delta_0 = 0.6$ K. We note that, compared with the C_p data ($H \parallel c$) shown in Fig. 1(b), the data in Fig. 10(a) have been adjusted by subtracting a linear term, $C_p(H) = k_L \cdot \mu_0 H$, where $k_L = 0.42$ mJ/K/T/mol-Cu. This subtraction was performed to correctly fit the Schottky anomaly, as the linear term is attributed to the YCOB kagome plane rather than the Schottky anomaly. C_{sc} quickly decays and becomes negligible when the field is higher than 10 T. To estimate the contribution of C_{ph}, we applied a Debye-Einstein function [25] to fit C_p versus T from 30 to 110 K:

$$3C_{\mathrm{ph}} = \frac{9RT^3}{\Theta_{\mathrm{D}}^3}\int_0^{\Theta_{\mathrm{D}}/T}\frac{\xi^4 e^{\xi}}{(e^{\xi}-1)^2}\mathrm{d}\xi + \frac{R}{T^2}\sum_{n=1}^{5}\frac{w_n\Theta_{\mathrm{En}}^2 e^{\Theta_{\mathrm{En}}/T}}{(e^{\Theta_{\mathrm{En}}/T}-1)^2}, \tag{A3}$$

where Θ_{D} and Θ_{En} are fitting parameters and w_n are the weights for different Θ_{En}. The fitting result and fitted parameters are shown in Fig. 10(b). The fitted C_{ph} was extended to low T and compared with the total specific heat in Fig. 10(c), which shows that C_{ph} is negligible when T is

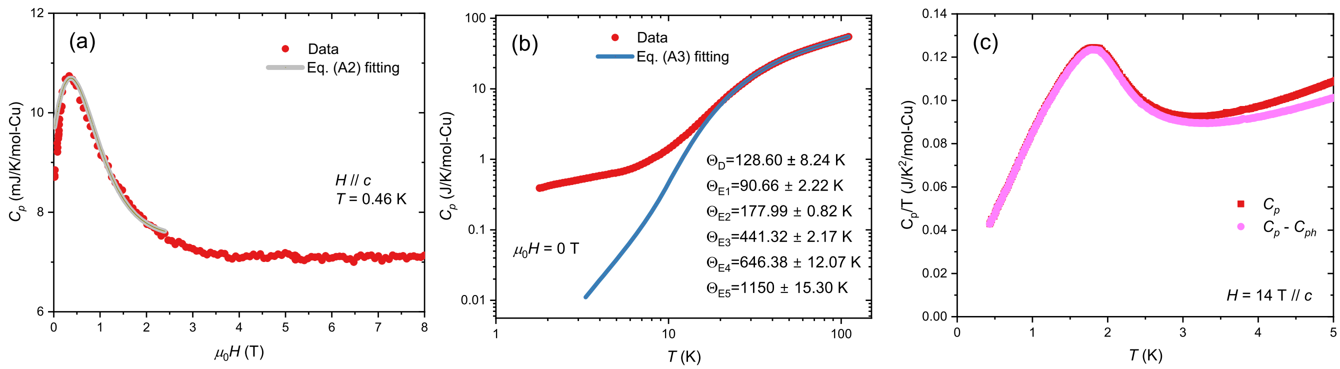

FIG. 10. Specific-heat contributions from Schottky and phonon terms. (a) The red dots represent the C_p data taken from Fig. 1(b) in the main text for $H \parallel c$ after subtracting a linear term $C_p(H) = k_L \cdot \mu_0 H$, where $k_L = 0.42$ mJ/K/T/mol-Cu. The gray curve is the Schottky contribution fitted using Eq. (A2) in the range of 0–2.5 T. (b) The red dots are the raw C_p data taken from 1.8 to 110 K at 0 T in the PPMS. The blue curve is the phononic specific heat fitted using Eq. (A3). The best-fit parameters are listed in the figure. (c) The red dots are the $\mu_0 H = 14$ T C_p data without subtracting the phonon contribution. The blue dots are the result of $C_p - C_{ph}$, i.e., a phonon contribution is subtracted from the red dots obtained from the fits in (b).

below 2 K. Therefore, we conclude that, in the region ($\mu_0 H > 10$ T, $T < 2$ K) that we focus on in this study, it should be safe to use the estimate $C_p \approx C_{\mathrm{ka}}$. High fields naturally separate the intrinsic specific-heat contributions induced by kagome frustrations from extrinsic localized excitation parts produced by orphan spins or band randomness [25,31,56] which have introduced controversial results in the ground state at zero field [24,25,30].

[1] P. W. Anderson, *Resonating valence bonds: A new kind of insulator?*, Mater. Res. Bull. **8**, 153 (1973).
[2] L. Savary and L. Balents, *Quantum spin liquids: A review*, Rep. Prog. Phys. **80**, 016502 (2016).
[3] Y. Zhou, K. Kanoda, and T.-K. Ng, *Quantum spin liquid states*, Rev. Mod. Phys. **89**, 025003 (2017).
[4] M. R. Norman, *Colloquium: Herbertsmithite and the search for the quantum spin liquid*, Rev. Mod. Phys. **88**, 041002 (2016).
[5] S. Yan, D. A. Huse, and S. R. White, *Spin-liquid ground state of the* $S = 1/2$ *kagome Heisenberg antiferromagnet*, Science **332**, 1173 (2011).
[6] R. Moessner and S. L. Sondhi, *Resonating valence bond phase in the triangular lattice quantum dimer model*, Phys. Rev. Lett. **86**, 1881 (2001).
[7] S. Depenbrock, I. P. McCulloch, and U. Schollwöck, *Nature of the spin-liquid ground state of the* $S = 1/2$ *Heisenberg model on the kagome lattice*, Phys. Rev. Lett. **109**, 067201 (2012).
[8] Y. Ran, M. Hermele, P. A. Lee, and X.-G. Wen, *Projected-wave-function study of the spin-*$1/2$ *Heisenberg model on the kagomé lattice*, Phys. Rev. Lett. **98**, 117205 (2007).
[9] Y. Iqbal, F. Becca, S. Sorella, and D. Poilblanc, *Gapless spin-liquid phase in the kagome spin-*$\frac{1}{2}$ *Heisenberg antiferromagnet*, Phys. Rev. B **87**, 060405(R) (2013).
[10] M. B. Hastings, *Dirac structure, RVB, and Goldstone modes in the kagomé antiferromagnet*, Phys. Rev. B **63**, 014413 (2000).
[11] Y.-C. He, M. P. Zaletel, M. Oshikawa, and F. Pollmann, *Signatures of Dirac cones in a DMRG study of the kagome Heisenberg model*, Phys. Rev. X **7**, 031020 (2017).
[12] S. Nishimoto, N. Shibata, and C. Hotta, *Controlling frustrated liquids and solids with an applied field in a kagome Heisenberg antiferromagnet*, Nat. Commun. **4**, 2287 (2013).
[13] D.-z. Fang, N. Xi, S.-J. Ran, and G. Su, *Nature of the* $1/9$*-magnetization plateau in the spin-*$\frac{1}{2}$ *kagome Heisenberg antiferromagnet*, Phys. Rev. B **107**, L220401 (2023).
[14] L.-W. He, S.-L. Yu, and J.-X. Li, *Variational Monte Carlo study of the* $1/9$*-magnetization plateau in kagome antiferromagnets*, Phys. Rev. Lett. **133**, 096501 (2024).
[15] M. P. Shores, E. A. Nytko, B. M. Bartlett, and D. G. Nocera, *A structurally perfect* $S = 1/2$ *kagomé antiferromagnet*, J. Am. Chem. Soc. **127**, 13462 (2005).
[16] T.-H. Han, J. S. Helton, S. Chu, D. G. Nocera, J. A. Rodriguez-Rivera, C. Broholm, and Y. S. Lee, *Fractionalized excitations in the spin-liquid state of a kagome-lattice antiferromagnet*, Nature (London) **492**, 406 (2012).
[17] D. E. Freedman *et al.*, *Site specific x-ray anomalous dispersion of the geometrically frustrated kagomé magnet, herbertsmithite,* $ZnCu_3(OH)_6Cl_2$, J. Am. Chem. Soc. **132**, 16185 (2010).
[18] Y. Y. Huang *et al.*, *Heat transport in herbertsmithite: Can a quantum spin liquid survive disorder?*, Phys. Rev. Lett. **127**, 267202 (2021).
[19] M. A. de Vries, K. V. Kamenev, W. A. Kockelmann, J. Sanchez-Benitez, and A. Harrison, *Magnetic ground state of an experimental* $S = 1/2$ *kagome antiferromagnet*, Phys. Rev. Lett. **100**, 157205 (2008).
[20] X.-H. Chen, Y.-X. Huang, Y. Pan, and J.-X. Mi, *Quantum spin liquid candidate* $YCu_3(OH)_6Br_2[Br_x(OH)_{1-x}]$ $(x \approx 0.51)$*: With an almost perfect kagomé layer*, J. Magn. Magn. Mater. **512**, 167066 (2020).
[21] Wei Sun, Ya-Xi Huang, Sergiy Nokhrin, Yuanming Pan, and Jin-Xiao Mi, *Perfect Kagomé lattices in* $YCu_3(OH)_6Cl_3$*: A new candidate for the quantum spin liquid state*, J. Mater. Chem. C **4**, 8772 (2016).

[22] A. Zorko, M. Pregelj, M. Klanjšek, M. Gomilšek, Z. Jagličić, J. S. Lord, J. A. T. Verezhak, T. Shang, W. Sun, and J.-X. Mi, *Coexistence of magnetic order and persistent spin dynamics in a quantum kagome antiferromagnet with no intersite mixing*, Phys. Rev. B **99**, 214441 (2019).

[23] O. Cépas, C. M. Fong, P. W. Leung, and C. Lhuillier, *Quantum phase transition induced by Dzyaloshinskii-Moriya interactions in the kagome antiferromagnet*, Phys. Rev. B **78**, 140405(R) (2008).

[24] Z. Zeng *et al.*, *Possible Dirac quantum spin liquid in the kagome quantum antiferromagnet* $YCu_3(OH)_6Br_2[Br_x(OH)_{1-x}]$, Phys. Rev. B **105**, L121109 (2022).

[25] J. Liu, L. Yuan, X. Li, B. Li, K. Zhao, H. Liao, and Y. Li, *Gapless spin liquid behavior in a kagome Heisenberg antiferromagnet with randomly distributed hexagons of alternate bonds*, Phys. Rev. B **105**, 024418 (2022).

[26] F. Lu, L. Yuan, J. Zhang, B. Li, Y. Luo, and Y. Li, *The observation of quantum fluctuations in a kagome Heisenberg antiferromagnet*, Commun. Phys. **5**, 272 (2022).

[27] S. Li *et al.*, *NMR evidence of spinon localization in the kagome antiferromagnet* $YCu_3(OH)_6Br_2[Br_{1-x}(OH)_x]$, Phys. Rev. B **109**, 104403 (2024).

[28] C. Lee, W. Lee, S. Lee, T. Yamanaka, S. Jeon, J. Khatua, H. Nojiri, and K.-Y. Choi, *Dirac spinons intermingled with singlet states in the random kagome antiferromagnet* $YCu_3(OD)_{6+x}Br_{3-x}(x = 0.5)$, Phys. Rev. B **110**, 064418 (2024).

[29] Z. Zeng *et al.*, *Spectral evidence for Dirac spinons in a kagome lattice antiferromagnet*, Nat. Phys. **20**, 1097 (2024).

[30] X. Hong, M. Behnami, L. Yuan, B. Li, W. Brenig, B. Büchner, Y. Li, and C. Hess, *Heat transport of the kagome Heisenberg quantum spin liquid candidate* $YCu_3(OH)_{6.5}Br_{2.5}$*: Localized magnetic excitations and a putative spin gap*, Phys. Rev. B **106**, L220406 (2022).

[31] B. S. Shivaram, J. C. Prestigiacomo, A. Xu, Z. Zeng, T. D. Ford, I. Kimchi, S. Li, and P. A. Lee, *Nonanalytic magnetic response and intrinsic ferromagnetic clusters in a kagome spin-liquid candidate*, Phys. Rev. B **110**, L121105 (2024).

[32] A. Xu *et al.*, *Magnetic ground states in the kagome system* $YCu_3(OH)_6[(Cl_xBr_{1-x})_{3-y}(OH)_y]$, Phys. Rev. B **110**, 085146 (2024).

[33] Itamar Kimchi, Adam Nahum, and T. Senthil, *Valence bonds in random quantum magnets: Theory and application to* $YbMgGaO_4$, Phys. Rev. X **8**, 031028 (2018).

[34] I. Kimchi, J. P. Sheckelton, T. M. McQueen, and P. A. Lee, *Scaling and data collapse from local moments in frustrated disordered quantum spin systems*, Nat. Commun. **9**, 4367 (2018).

[35] G. Zheng *et al.*, *Unconventional magnetic oscillations in kagome Mott insulators*, Proc. Natl. Acad. Sci. U.S.A. **122**, e2421390122 (2025).

[36] S. Jeon *et al.*, *One-ninth magnetization plateau stabilized by spin entanglement in a kagome antiferromagnet*, Nat. Phys. **20**, 435 (2024).

[37] S. Suetsugu *et al.*, *Emergent spin-gapped magnetization plateaus in a spin-*$1/2$ *perfect kagome antiferromagnet*, Phys. Rev. Lett. **132**, 226701 (2024).

[38] P. A. Goddard, J. Singleton, A. L. Lima-Sharma, E. Morosan, S. J. Blundell, S. L. Bud'ko, and P. C. Canfield, *Separation of energy scales in the kagome antiferromagnet* TmAgGe*: A magnetic-field-orientation study up to 55 T*, Phys. Rev. B **75**, 094426 (2007).

[39] P. A. Goddard *et al.*, *Experimentally determining the exchange parameters of quasi-two-dimensional Heisenberg magnets*, New J. Phys. **10**, 083025 (2008).

[40] S. Tagliati, V. M. Krasnov, and A. Rydh, *Differential membrane-based nanocalorimeter for high-resolution measurements of low-temperature specific heat*, Rev. Sci. Instrum. **83**, 055107 (2012).

[41] P. F. Sullivan and G. Seidel, *Steady-state, ac-temperature calorimetry*, Phys. Rev. **173**, 679 (1968).

[42] M. K. Ray, K. Bagani, P. K. Mukhopadhyay, and S. Banerjee, *Origin of cluster spin glass and nuclear Schottky anomaly in* $Mn_{50}Ni_{38.5}Sn_{11.5}$ *alloy*, Europhys. Lett. **109**, 47006 (2015).

[43] J. Sheng *et al.*, *Two-dimensional quantum universality in the spin-*$1/2$ *triangular-lattice quantum antiferromagnet* $Na_2BaCo(PO_4)_2$, Proc. Natl. Acad. Sci. U.S.A. **119**, e2211193119 (2022).

[44] Z. Zou and P. W. Anderson, *Effective magnetic moments of heavy fermions and the Wilson ratio for Kondo lattices*, Phys. Rev. Lett. **57**, 2073 (1986).

[45] E. M. Brüning, C. Krellner, M. Baenitz, A. Jesche, F. Steglich, and C. Geibel, CeFePO*: A heavy fermion metal with ferromagnetic correlations*, Phys. Rev. Lett. **101**, 117206 (2008).

[46] Z. Yang *et al.*, *Unveiling the double-peak structure of quantum oscillations in the specific heat*, Nat. Commun. **14**, 7006 (2023).

[47] Y. Aoki *et al.*, *Thermal properties of metamagnetic transition in heavy-fermion systems*, J. Magn. Magn. Mater. **177–181**, 271 (1998).

[48] Z. Yang *et al.*, *Evidence for large thermodynamic signatures of in-gap fermionic quasiparticle states in a Kondo insulator*, Nat. Commun. **15**, 7801 (2024).

[49] A. H. Castro Neto, F. Guinea, N. M. R. Peres, K. S. Novoselov, and A. K. Geim, *The electronic properties of graphene*, Rev. Mod. Phys. **81**, 109 (2009).

[50] S. Yamashita, Y. Nakazawa, M. Oguni, Y. Oshima, H. Nojiri, Y. Shimizu, K. Miyagawa, and K. Kanoda, *Thermodynamic properties of a spin-*$1/2$ *spin-liquid state in a* κ*-type organic salt*, Nat. Phys. **4**, 459 (2008).

[51] S. Yamashita, T. Yamamoto, Y. Nakazawa, M. Tamura, and R. Kato, *Gapless spin liquid of an organic triangular compound evidenced by thermodynamic measurements*, Nat. Commun. **2**, 275 (2011).

[52] Byungmin Kang and Patrick A. Lee, *Generation of gauge magnetic fields in a kagome spin liquid candidate using the Dzyaloshinskii-Moriya interaction*, Phys. Rev. B **109**, L201104 (2024).

[53] Q. Barthélemy *et al.*, *Specific heat of the kagome antiferromagnet herbertsmithite in high magnetic fields*, Phys. Rev. X **12**, 011014 (2022).

[54] T.-H. Han, R. Chisnell, C. J. Bonnoit, D. E. Freedman, V. S. Zapf, N. Harrison, D. G. Nocera, Y. Takano, and Y. S. Lee, *Thermodynamic properties of the quantum spin liquid candidate* $ZnCu_3(OH)_6Cl_2$ *in high magnetic fields*, arXiv:1402.2693.

[55] T. Radu, H. Wilhelm, V. Yushankhai, D. Kovrizhin, R. Coldea, Z. Tylczynski, T. Lühmann, and F. Steglich, *Bose-Einstein condensation of magnons in* Cs_2CuCl_4, Phys. Rev. Lett. **95**, 127202 (2005).

[56] H. Kawamura, K. Watanabe, and T. Shimokawa, *Quantum spin-liquid behavior in the spin*-$1/2$ *random-bond Heisenberg antiferromagnet on the kagome lattice*, J. Phys. Soc. Jpn. **83**, 103704 (2014).